



Propagation of magnetic charge monopoles and Dirac flux strings in an artificial spin-ice lattice

S. D. Pollard,^{1,2} V. Volkov,¹ and Y. Zhu^{1,2,*}

¹*Department of Condensed Matter Physics, Brookhaven National Laboratory, Upton, New York 11973, USA*

²*Department of Physics, Stony Brook University, Stony Brook, New York 11794, USA*

(Received 18 November 2011; published 4 May 2012)

We systematically investigate magnetic reversal of permalloy islands in a square spin-ice geometry with *in situ* Lorentz microscopy. Differential phase imaging reveals the presence of a flux channel similar to a Dirac string between the magnetic charge monopoles during the reversal. Analysis of the phase images shows that positively and negatively charged monopoles always move together with the flux channel. Statistical analysis of monopole populations and system correlations shows the emergence of a highly frustrated state for low magnetizations. This state is explained by a strong influence of charge ordering, which limits monopole densities.

DOI: [10.1103/PhysRevB.85.180402](https://doi.org/10.1103/PhysRevB.85.180402)

PACS number(s): 75.25.-j, 75.60.Jk, 75.75.-c, 85.75.-d

Spin ices have received a great deal of attention in recent years due to many interesting effects that arise from their intrinsic magnetic frustration, such as the emergence of magnetic charges and monopole-like quasiparticles.^{1,2} These are coupled in pairs via a Dirac string, which act as a flux channel for the charges, preserving Maxwell's equations. In spin ices, the magnetic moments within a lattice obey "ice" rules analogous to the ice rule for solid water. In traditional spin-ice materials, this effect occurs in three-dimensional crystal lattices.^{2,3} Recently, two dimensional, macroscopic analogs have been studied using thin films of lithographically patterned rectangular magnetic islands.⁴⁻¹⁵ Due to shape anisotropy, the magnetic moment of each island lies predominantly along the long axis, allowing for each island to be approximated as an Ising spin. The new size scale and simple fabrication methods of these two-dimensional analogs allow for experimentally controllable geometries, along with direct imaging of local moment configurations and open a new regime in which frustration physics can be directly studied.

Great interest has recently been focused on studying the various ordering processes in which frustration arises in these systems, whether by application of a standard ac-demagnetization cycle^{4,6,7,9-11,13,14,16} or, more recently, in fabricated states that are thermally ordered.¹¹ Additionally, the kagome lattice has been used to study the motion of monopoles within the lattice, which, due to the lattice topology, exhibit a dimensional reduction in their propagation, leading to the trapping of monopole charges within the lattice. These studies have used a dc magnetic field in order to excite the monopoles from an initially polarized state.^{7,10} In this work, using Lorentz microscopy and phase retrieval methods, we examine *in situ* both nucleation and propagation of magnetic charges, or monopoles by the dc magnetization method in the magnetic square-lattice geometry. The lattice diagonal direction, hereafter referred to as the [11] direction, was chosen in order to exploit the asymmetric coupling between all neighboring elements in order to coerce a quasiground, low-magnetization state.

Electron-beam lithography using a spin-coated ZEP (copolymer chloromethacrylate/methylstyrene) resist followed by electron-beam evaporation was used to fabricate 14×14 vertex "square-ice" arrays (a total of 420 elements)

of 100-nm-wide, 300-nm-long, and 30-nm-thick permalloy elements with a lattice constant of 450 nm and an "open" edge boundary [Fig. 1(a)]. A field-emission 300-kV transmission electron microscope (JEM3000F) was used for *in situ* magnetization experiments of the square spin-ice lattice. For analysis of magnetic domains and spin configurations we used a Fresnel imaging mode followed by phase retrieval methods based on the transport-of-intensity equation (TIE) approach.¹⁷⁻¹⁹ The magnetic field of the microscope perpendicular to the specimen plane was carefully calibrated, and its magnitude was controlled by varying the objective lens current.²⁰ Field reversal cycles were completed by tilting the sample in the residual out-of-plane magnetic field. The sample was initially polarized along the [11] direction, then switched to the opposite [-1-1] direction, and finally returned to the original state. An ac demagnetization alternately switches elements along the [01] and [10] axis, coercing the system toward its ground state, until it is jammed in a highly frustrated state which strongly obeys local ice rules, as observed in recent work by Phatak *et al.*¹⁴ in which the ordering appears to be moderated by the propagation of monopole-type defect pairs. These pairs are connected by chains of switched elements reminiscent of Dirac strings. The [11] reversal differs by allowing switching along both axes simultaneously and exploits the asymmetric coupling between elements at a vertex. Our experimental setup and Lorentz phase imaging allowed for direct observations of local moment configurations [Figs. 1(a) and 1(b)] and the fringing field of the elements at different field strengths during the reversal, and through image sequences, various system parameters commonly used to characterize these systems, such as correlation functions, vertex populations [Fig. 1(c)], and the reversal fraction of elements, were determined [Fig. 1(d)]. Such a thorough analysis has been lacking in previous works and is essential to understanding the details of the ordering process within these systems. Through these statistical measurements and real-space observations, we were able to determine how the coupling acts to locally enforce the ice rules in the systems during reversal cycles.

Additionally, we performed numerical simulations in which the individual moments are treated as point dipoles with an assigned critical switching field.⁴ The large size of arrays studied in the system means that full-scale micromagnetic

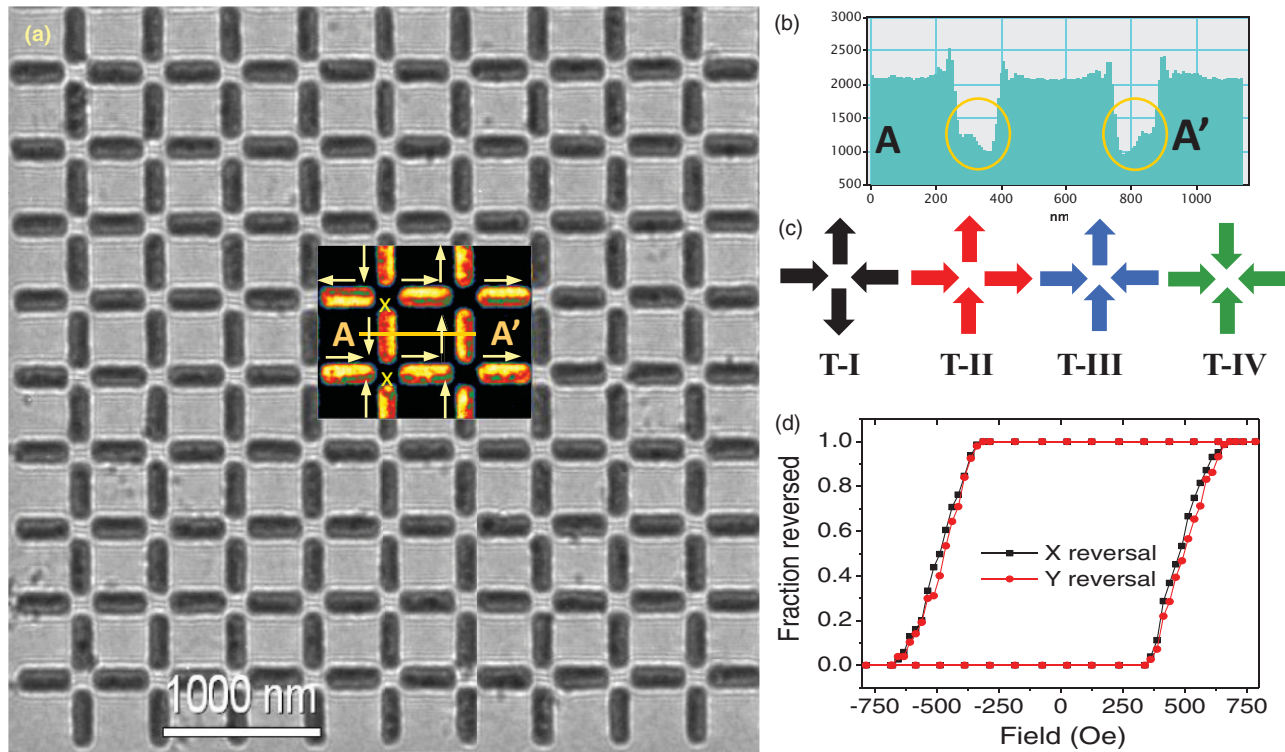


FIG. 1. (Color) (a) Lorentz image of a typical section of the 420-permalloy-element artificial square spin-ice array. The inset shows in color code the enhanced inverse contrast. For clarity, local moment directions of the elements are marked by arrows, and ice-rule-violating configurations are denoted by crosses. (b) Local line profile across two parallel elements A-A' in (a) showing opposite moment configurations as follows from the asymmetry in the intensity profile (marked by the circles). (c) The four possible topological vertex types. Only types T-I and T-II satisfy the ice rules (two in/two out), while T-III and T-IV do not. (d) Fraction of the elements in the entire array switched along the basal axis as a function of applied field.

calculations cannot feasibly be carried out. Meanwhile, the point-dipole-approximation method provides a computationally effective verification of the observed results along with dynamical evolution details of the system not easily accessed experimentally. In these simulations the magnetization of each dipole was determined using the standard properties of permalloy and magnetic-island geometry. Critical fields were obtained experimentally [Fig. 1(d)] and were modeled by the Gaussian distribution, centered at 320 Oe with a 60 Oe variation (along the element's long axis). In the computational model we assumed that the critical switching field ($H_{c,i}$) of the i th element follows from the condition $H_{\text{ext}} + \sum H_{ij} > H_{c,i}$, where H_{ext} is the external magnetic field component along the (x, y) axes of the i th element. The summation is performed over dipolar fields from all j th elements relative to the i th element of interest, assuming that $i \neq j$. In order to account for field misalignment, we determined an offset of 2° from the $[11]$ axis.

From a geometric point of view we can group sets of islands shown by static Lorentz images in Fig. 1(a) into four possible vertex types, labeled as type I (T-I) through type IV (T-IV) in order of increasing vertex energy.^{4,5,16} Only the T-I and T-II vertices [Fig. 1(c)] have formal zero balance of magnetic charges ($+2q/-2q$) for two pairs of magnetic elements pointed in (positive)/out (negative) or at a single vertex, obeying the “two-in/two-out” ice rule leading to the lowest vertex energy. Other vertices, T-III and T-IV,

with formal magnetic charges $+3q/-1q$ and $+4q/0q$ created by vectors pointing in/out, apparently violate the “ice rule” and therefore will have a higher vertex energy with excessive magnetic charges $+2q$ and $+4q$. We expect them to behave as magnetic “monopoles,” and they are termed monopole charges. In particular, our TEM data show the systematic absence of T-IV vertices, in agreement with the highest energy for such a vertex configuration. Therefore, we shall discuss further only the population statistics for T-I, T-II, and T-III vertices during the reversal process.

To reveal the intriguing frustration physics of magnetic switching in the spin-ice lattice, the sample was magnetized and demagnetized *in situ* and examined using Lorentz microscopy. We focused on the interaction and correlations of the neighboring elements by observing their in-plane fringing field using Lorentz phase microscopy based on differential phase imaging [differential transport of intensity (DTIE); see the Supplemental Material²²]. The ability to see the in-plane distribution of magnetic flux and fringing field that connect the neighboring elements, which was impossible using magnetic force microscopy (MFM) imaging, is crucial to our advancement in understanding the reversal processes in frustrated spin-ice systems. Figure 2 gives an example of DTIE showing the change of magnetic flux distribution, after electrostatic potential subtraction, during the partial demagnetization (363 Oe) along the $[11]$ direction from the initial polarized state. Complementary Lorentz microscopy was also used for

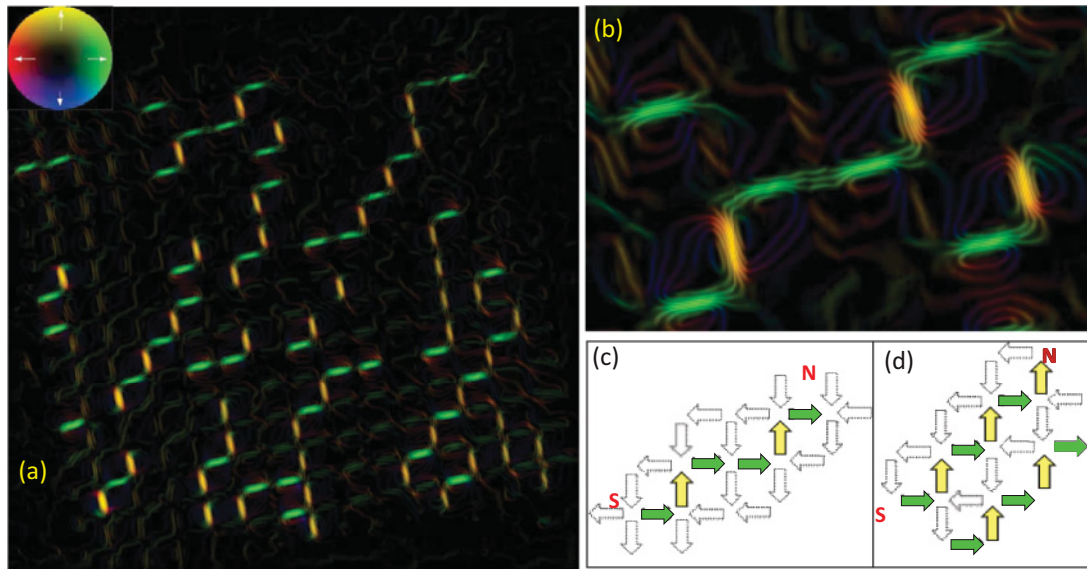


FIG. 2. (Color) (a) Difference map of magnetic flux distribution between the partial demagnetized state under 363-Oe applied field and the initial polarized state, showing individual chains of switched elements using the differential phase imaging method. Here the cosine of the magnetic phase map representing flux density changes is overlaid with magnetization induction map shown by the color vector wheel. (b) A magnified area of (a) showing a single chain of switched elements and the associated leakage flux distribution. The switched elements behave as flux channels, or Dirac strings, between the magnetic charges at the two ends of the chain. The terminating points are T-III charged vertices. (c) Schematic of magnetic switching shown in (b), illustrating the propagation of Dirac strings (the chain of colored arrows) joining two moving away S/N monopoles and a local defect (indicated by two neighboring green arrows). Initial nonswitching elements are shown by grey arrows in (c) and (d) and as a dark background in (a) and (b). (d) The ideal AFM-ordered structure of zero net magnetization expected for regular propagation of steplike Dirac strings. This ordering is blocked by frustration and disorder within the lattice. Apparently, such an ideal AFM-ordered ground state is not always easy to achieve in a demagnetized state of the spin-ice lattice.

dynamic observation and statistical analysis of the reversal process of several hundreds of magnetic elements (Fig. 1) to estimate the net magnetization of the system and correlation statistics for 16 possible moment configurations on each vertex formed by four adjacent elements [Fig. 1(c)]. We note that the reversal begins with the switching of single elements, creating pairs of oppositely charged T-III monopoles, which are labeled in Fig. 2(c) as S and N poles, and corresponds to the initial rise in T-III populations in Fig. 3(a). As the field increases, both S and N poles move away from each other by leaving behind a string of magnetically switched elements [Figs. 2(b) and 2(c)]. Similar to Dirac's flux strings,²² these strings, or channels, carry conservative magnetic flux between the stretched S and N poles, existing exclusively as T-III vertices [Fig. 2(a) and 2(b)]. While hypothesized to exist in this system in Ref. 14, the identification of chains of switched elements as Dirac strings was impossible due to the presence of background magnetic flux. This is a result of the charges and associated strings being excitations on top of a polarized state, which is subtracted in DTIE but not in conventional techniques.

With the increase of the applied field, the density of these poles in the lattice grows [Fig. 3(a)], along with populations of T-I vertices, corresponding to local ground-state ordering, at the expense of T-II vertex populations. As larger fields are applied, both T-III and T-I vertex populations fall, and T-II populations grow. The largest relative populations of T-I vertices and the highest degree of ground-state ordering appear at low net magnetizations, near the middle of the reversal cycle [Figs. 3(b) and 3(c)]. The degree of ground-state ordering

is quantified using the correlations introduced in Refs. 6 and 16 and is given for the three types of nearest-neighbor interactions, defined in the inset of Fig. 3(c). The significant growth in short-range correlations [Fig. 3(c)] along with T-I vertex populations [Figs. 3(a) and 3(b)] indicates a high degree of local ordering. It should be noted that all higher-order correlations are approximately 0 at small values of M/M_s , indicating that long-range frustration also plays a significant role in the system dynamics. Simulated results are in good agreement with experimental observations outside of a small excess of T-III populations for low net magnetizations. This is most likely due to deficiencies in the point-dipole model described in Ref. 11.

The high degree of ordering is a result of the asymmetric coupling between neighboring elements and leads to a preferential motion of a monopole along the alternating axis and the field direction, indicative of low-energy T-I vertex growth (Figs. 2 and 4). We observe that T-I vertices exceed the random switching case (see Supplemental Material²¹) by almost 30% at the midpoint of the reversal [Fig. 3(a)]. More interestingly, T-III vertex populations also show a deficit of nearly 30% and appear to saturate below net magnetizations of 0.5 [Fig. 3(c)]. This saturation can be largely understood by the interactions of neighboring monopoles. For example, when oppositely charged monopoles occupy neighboring lattice sites, there is a large attractive interaction between the two. If the monopoles subsequently move to the same lattice site, they are annihilated. This annihilation process results in the merging of the two corresponding flux channels. By looking at what happens to

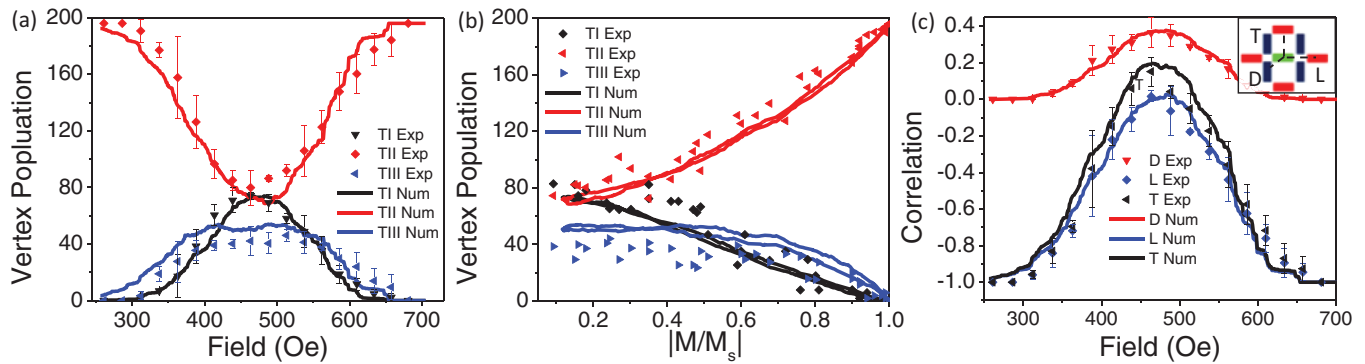


FIG. 3. (Color) (a) Vertex populations as a function of applied field. (b) Vertex populations as a function of normalized net magnetization (M/M_s). Data points are shown for four different samples during a reversal cycle. In both experimental and numerical results, T-III populations saturate below a net magnetization of about 0.5. (c) Correlation effects as a function of applied field. In all plots experimental data are shown by discrete symbols, while theoretical calculations are shown by solid lines of the appropriate color.

adjacent charges in sequential Lorentz images, we observe this annihilation process occurs 74% of the time that this transition is topologically allowable. This represents a large increase from what would be expected in a noninteracting system. Similar observations of attractive and repulsive interactions were recently seen in thermally ordered samples, which imposed limitations on monopole densities within domains and along excitations.¹¹ Further evidence of these interactions

is demonstrated by the lack of T-IV vertices at any step during the reversal. Simulations indicate that they do not exist even as transient states, which would indicate two monopoles of similar sign occupying the same lattice site. These observations suggest a strong influence of charge ordering during the reversal, in which interactions are responsible for imposing a maximal limit of monopole densities and act to locally enforce the ice rules. Evidence of weak charge ordering was also seen in recent work on a similar system in Ref. 5. This ordering process is in sharp contrast to that observed in the kagome lattice. In the kagome lattice, dimensional reduction is observed, which causes the monopoles to move in 1D “cascades.” The dimensional reduction prevents monopoles from crossing other Dirac strings as well as ensures that at the end of the reversal every lattice site is populated by an emergent monopole, in which case no saturation occurs.

In summary, we show that the magnetic reversal process of an artificial spin-ice lattice is associated with nucleation, propagation, and annihilation of magnetic charges, or monopoles. The utility in Lorentz microscopy and phase imaging in these systems allows for the subtraction of extraneous electrostatic and background magnetic potentials that preclude direct imaging and hence identification of Dirac strings which couple individual magnetic excitations. All monopoles unexceptionally were nucleating and annihilating in pairs of S/N poles and coupled with magnetic flux channels, or Dirac strings. They remain conservative, in accordance with Maxwell’s equations, during propagation for the reversal process via flux channels with opposite signs. We also demonstrate that these magnetic charges behave as individual monopole/antimonopole (S/N) pairs with distinct signs of interactions that govern the evolution of vertex populations and ordering under application of fields. Specifically, a saturation of monopole density within the lattice results from the repulsive and attractive interaction between these individual charges which locally enforces the ice rules. Furthermore, statistical analysis reveals the growth of ground-state ordering that is blocked at larger length scales, indicating a highly frustrated intermediate state. This state of order resulting from field application along this symmetry axis was recently suggested,⁵ but it has not been experimentally shown until now.

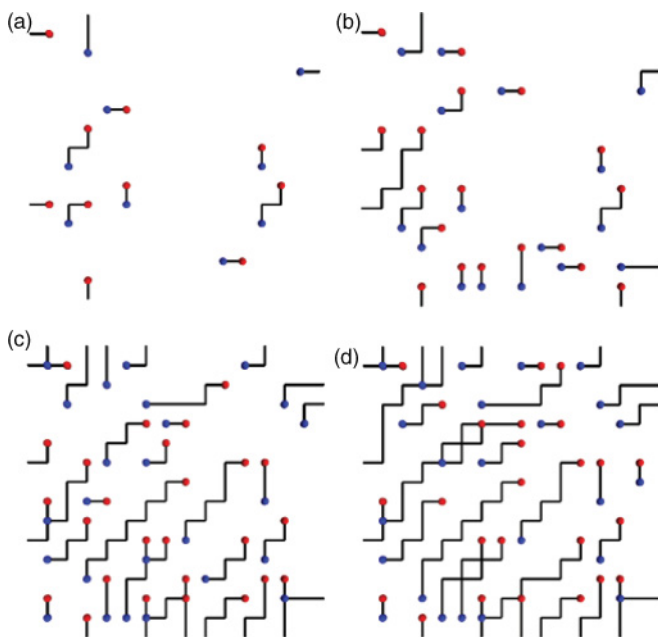


FIG. 4. (Color) Diagram of the switching process in the square spin-ice lattice. The field was applied along the [11] direction. The switching was reconstructed from consecutive Lorentz images recorded for applied magnetic field of (a) 337, (b) 363, (c) 388, and (d) 413 Oe. Switched elements are shown in black, while unswitched elements are removed for clarity. Positive (negative) charges are denoted by red (blue) circles. The growth of density and chain length is clearly visible from (a) to (d). The steplike pattern that emerges is a result of the asymmetric coupling by flux channels between paired vertices or monopoles and indicates large T-I vertex populations. All chains terminate at the lattice edges.

This work was carried out in part at the Center for Functional Nanomaterials, Brookhaven National Laboratory, and was supported by the US Department of Energy, Office of Basic Energy Science, Material Sci-

ences and Engineering Division, under Contract No. DE-AC02-98CH10886. The authors acknowledge J. P. Morgan, Z. Budrikis, and C. H. Marrows for useful discussions.

*Corresponding author: zhu@bnl.gov

- ¹C. Castelnovo, R. Moessner, and S. L. Sondhi, *Nature (London)* **451**, 42 (2008).
- ²A. P. Ramirez, A. Hayashi, R. J. Cava, R. Siddharthan, and B. S. Shastry, *Nature (London)* **399**, 333 (1999).
- ³S. T. Bramwell and M. J. P. Gingras, *Science* **294**, 1495 (2001).
- ⁴Z. Budrikis, P. Politi, and R. L. Stamps, *Phys. Rev. Lett.* **105**, 017201 (2010).
- ⁵J. P. Morgan, A. Stein, S. Langridge, and C. H. Marrows, *New J. Phys.* **13**, 105002 (2011).
- ⁶X. Ke, J. Li, C. Nisoli, P. E. Lammert, W. McConville, R. F. Wang, V. H. Crespi, and P. Schiffer, *Phys. Rev. Lett.* **101**, 037205 (2008).
- ⁷S. Ladak, D. E. Read, G. K. Perkins, L. F. Cohen, and W. R. Branford, *Nat. Phys.* **6**, 359 (2010).
- ⁸P. E. Lammert, X. Ke, J. Li, C. Nisoli, D. M. Girand, V. Crespi, and P. Schiffer, *Nat. Phys.* **6**, 786 (2010).
- ⁹E. Mengotti, L. J. Heyderman, A. Fraile Rodriguez, A. Bisig, L. Le Guyader, F. Nolting, and H. B. Braun, *Phys. Rev. B* **78**, 144402 (2008).
- ¹⁰E. Mengotti, L. J. Heyderman, A. F. Rodriguez, F. Nolting, R. M. Hügli, and H. Braun, *Nat. Phys.* **7**, 68 (2011).
- ¹¹J. P. Morgan, A. Stein, S. Langridge, and C. H. Marrows, *Nat. Phys.* **7**, 75 (2011).
- ¹²C. Nisoli, J. Li, X. Ke, D. Garand, P. Schiffer, and V. H. Crespi, *Phys. Rev. Lett.* **105**, 047205 (2010).
- ¹³C. Nisoli, R. Wang, J. Li, W. F. McConville, P. E. Lammert, P. Schiffer, and V. H. Crespi, *Phys. Rev. Lett.* **98**, 217203 (2007).
- ¹⁴C. Phatak, A. K. Petford-Long, O. Heinonen, M. Tanase, and M. De Graef, *Phys. Rev. B* **83**, 174431 (2011).
- ¹⁵Y. Qi, T. Brintlinger, and J. Cumings, *Phys. Rev. B* **77**, 094418 (2008).
- ¹⁶R. F. Wang *et al.*, *Nature (London)* **446**, 102 (2007).
- ¹⁷V. V. Volkov and Y. Zhu, *Phys. Rev. Lett.* **91**, 043904 (2003).
- ¹⁸V. V. Volkov and Y. Zhu, *Ultramicroscopy* **98**, 271 (2004).
- ¹⁹S. Bajt, K. A. Nugent, M. McCartney, M. Wall, and D. Paganin, *Ultramicroscopy* **83**, 67 (2000).
- ²⁰V. V. Volkov, D. C. Crew, Y. Zhu, and L. H. Lewis, *Rev. Sci. Instrum.* **73**, 2298 (2002).
- ²¹See Supplemental Material at <http://link.aps.org/supplemental/10.1103/PhysRevB.85.180402> for derivation of the differential TIE method, as well as details of the numerical simulations and simulated results for a decoupled system.
- ²²P. A. M. Dirac, *Proc. R. Soc. London, Ser. A* **133**, 60 (1931).